AIP Advances

Evidence for the suppression of intermediate anti-ferroelectric ordering and observation of hardening mechanism in $Na_{1/2}Bi_{1/2}TiO_3$ ceramics through cobalt substitution

Cite as: AIP Advances **4**, 017111 (2014); https://doi.org/10.1063/1.4862169
Submitted: 10 December 2013 • Accepted: 31 December 2013 • Published Online: 09 January 2014

Karthik Thangavelu, Ranjith Ramadurai and Saket Asthana

Evidence for the suppression of intermediate anti-ferroelectric ordering and observation of hardening mechanism in $Na_{1/2}Bi_{1/2}TiO_3$ ceramics through cobalt substitution

Karthik Thangavelu,[1,2] Ranjith Ramadurai,[2] and Saket Asthana[1,a]
[1]*Advanced Functional Materials Laboratory, Department of Physics, Indian Institute of Technology Hyderabad, Andhra Pradesh - 502 205, India.*
[2]*Department of Materials Science and Engineering, Indian Institute of Technology Hyderabad, Andhra Pradesh - 502 205, India.*

(Received 10 December 2013; accepted 31 December 2013; published online 9 January 2014)

Co-ion (*5 mol %*) substitution in $Na_{1/2}Bi_{1/2}TiO_3$ (NBT) host lattice and their effects on the structural, ferroelectric and dielectric behavior has been investigated thoroughly in this present study. The substituted Co-ion at Ti-site acts an acceptor type doping and hardens (*i.e., increase in coercivity*) the system without any noticeable change in the remanent polarization values. However, the intermediate antiferroelectric (AFE) ordering which exists between 200 °C–280 °C in NBT system has been suppressed due to Co-ion substitution, which is an interesting feature for device applications. [http://dx.doi.org/10.1063/1.4862169]

I. INTRODUCTION

In the recent years, $Na_{0.5}Bi_{0.5}TiO_3$ (NBT) and its solid solution based perovskite system has been well studied because of its exceptionally high electro-strain.[1,2] It has triggered the scientific/technological community to look beyond classical Pb-based perovskite systems due to its environmental issues.[2] Apart from the application point of view, NBT being an A-site disordered system with long range ferroelectric ordering[3] display several structural phase transitions within room temperature to 545 °C.[4,5] In addition, the presence of heterovalent A-site cation disorder and their hetero polar nature is believed to give rise for relaxor features in NBT.[6–9] The aforementioned features made them unique from other B-site disordered system such as PMN, PMN-PT etc.[10] It is well known from x-ray/neutron diffraction experiments, on cooling from high temperature prototypic cubic phase ($Pm\bar{3}m$) it pass through a tetragonal phase i.e., *P4bm* ($a^0a^0c^+$) between ~540 °C–300 °C and stabilizes in *R3c* symmetry ($a^-a^-a^-$ tilt system) at room temperature via an intermediate (i.e., 200–280 °C) modulated structure with antiferroelectric (AFE) ordering.[4,5] The presence of AFE ordering has been confirmed by observation of a dielectric anomaly around 200 °C[6,7] and exhibited a double hysteresis (P-E) loop,[8,11,12] which is an unique character of an AFE-ordering. Though the origin of such strain modulated structure with AFE characteristics remains ambiguous, it is expected to arise due to the formation of stacking fault structures between 200 °C–280 °C. The structural analysis of the intermediate AFE phase was resolved by Dorcet *et al.*[13] using high temperature transmission electron microscopic (TEM) studies. It was observed that NBT possess a modulated *Pnma* phase co-existing with the *R3c* phase in the intermediate temperature regime as mentioned above.[14] However, there are several reports addressing the room temperature crystal structure of NBT as monoclinic (*Cc*);[15–17] in addition a new phase transition sequence has been reported by

[a]Author for Correspondence: asthanas@iith.ac.in

Aksel *et al.*[18] However, there has not been any extensive studies carried out on the origin of AFE ordering in NBT at intermediate temperatures (200–280 °C). In addition presence of such additional ordering prior to the FE phase transition is not preferred from the application point of view in functional ceramics. Hence, understanding the origin of such coexisting modulated structure is crucial in order to suppress/surpass the additional phase transition considering the utilization of NBT for practical purposes. Hence, in this manuscript we address the origin of AFE phase and suppression of the same through aliovalent substitution in B-site. In order to match the cationic radius, to avoid charged defect formation and to retain the ferroelectric activeness of the B-site cation, Co was chosen as a suitable candidate for B-Site substitution in NBT ceramics. Though there are few reports at B-site substitution in NBT with Mn and Fe, no specific change in the AFE ordering/behavior was observed or reported.[19,20]

II. EXPERIMENTAL DETAILS

Polycrystalline $Na_{0.5}Bi_{0.5}TiO_3$ (NBT) and $Na_{0.5}Bi_{0.5}Ti_{0.95}Co_{0.05}O_{3\pm\delta}$ (NBT-Co) samples were prepared by using conventional solid state reaction technique with Bi_2O_3, Na_2CO_3, TiO_2 and CoO (99.99% Sigma Aldrich Chemicals) as precursors. The calcined phase pure powders were pelletized followed by sintering in atmospheric conditions at 1150 °C/3hrs for NBT and 1100 °C/3hrs for NBT-Co samples. The structural studies were carried out using a powder diffractometer (PANlytical X'pert pro). The analysis of the diffraction patterns were carried out using FULLPROF software package.[21] Diffuse reflectance spectroscopy (DRS) on the powder samples were recorded using UV-Vis-NIR spectrophotometer (Shimadzu-UV3600) in the wavelength range from 200 nm–1800 nm with a wavelength accuracy of ±1 nm resolution. The phonon modes were recorded using a Laser Micro Raman spectrometer (Bruker, Senterra) in a back–scattering geometry equipped with an excitation source of 532 nm and 10 mW power. FE-SEM micrographs and elemental mapping on the surface of sintered samples were performed using Carl Zeiss, Supra-40. Polarization (P) vs. Electric field (E) hysteresis measurements were carried out using aix-ACCT systems (TF analyzer-2000) on silver electroded samples. High temperature dielectric measurements were performed in a precision Impedance Analyzer (Wayne-Kerr-6500B) with a heating rate of 0.5 °C /min and data were collected for every 5 °C interval.

III. RESULTS AND DISCUSSION

Phase analysis of the sintered NBT and NBT-Co samples were refined by considering *R3c* space group. In the refinement process, the background was estimated by linear interpolation between two fixed values and peak shapes were described by using pseudo-voigt function.[22] Both NBT and NBT-Co, XRD-patterns fit well with the *R3c* model depicting their single phase characteristics (see Fig. 1(a) and 1(b)). Further, no other secondary phases were observed in both the samples within the detection limit of powder diffractometer.

The presence of $1/2(ooo)$ Bragg reflections (see insets of Fig. 1(a) and 1(b)) in both NBT and NBT-Co samples indicate the presence of antiphase tilt system (i.e., $a^-a^-a^-$), which is accordance with the existing reports.[4,6,9] In addition, the lattice parameters extracted from the refinement studies indicate a clear variation in the lattice parameters due to Co substitution. The variation in Bragg peak position (i.e., $\Delta 2\theta$) accompanied with a shift towards lower degree of $\geq$3% observed in (024) plane (See Fig. 1(c) and 1(d)) further supports the unit-cell expansion in NBT-Co system. Though the shift in peak positions to lower degree was commonly observed, the magnitude of shift was found to be maximum in the peaks corresponding to Ti-O plane (*NBT: $a = 5.4818(4)$ Å; $c = 13.4910(2)$ Å; $V = 351.09$ (Å)^3, NBT-Co: $a = 5.4934(5)$ Å; $c = 13.5142(2)$ Å; $V = 353.18$ (Å)^3*). This increase in d-spacing/unit-cell volume could be attributed to the incorporation of larger ionic radii Co^{2+} -ion at Ti-site of the NBT host lattice (*$Ti^{4+} = 0.605$Å; $Co^{2+} = 0.745$Å; $Co^{3+} = 0.61$Å; $Co^{4+} = 0.53$Å*), which will be discussed further below. The incorporation of Co^{2+}-ions is being compensated with the formation of oxygen vacancies to maintain charge neutrality as follows: $CoO \xrightarrow{TiO_2} Co''_{Ti} + O^{\times}_{O} + V^{\bullet\bullet}_{O}$.[23,24] However, Co is known to stabilize under mixed oxidation

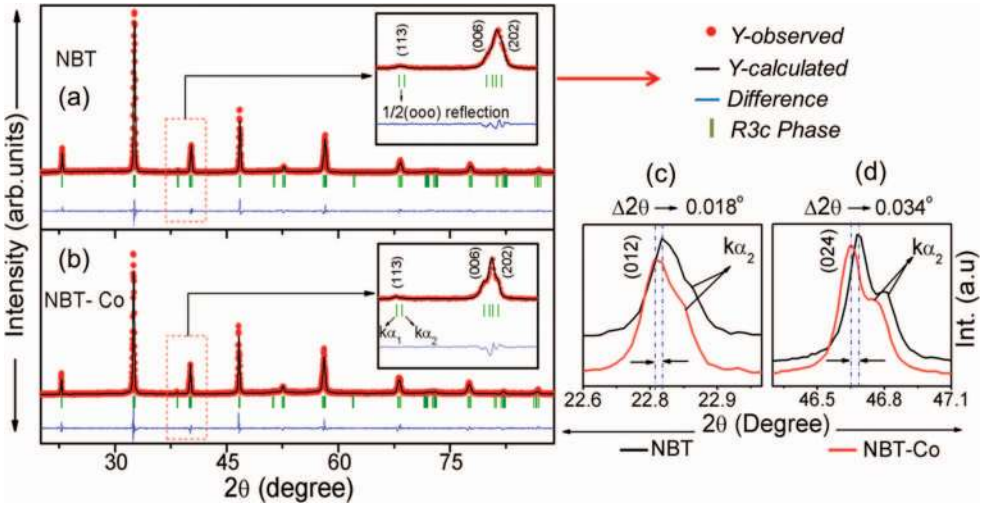

FIG. 1. Reitveld refined room temperature XRD patterns of (a) NBT and (b) NBT-Co samples, with inset showing the magnified region as an indicator of goodness of fit. (c) & (d) Close observation of selected Bragg reflections indicating the shift in 2θ positions due to Cobalt-ion substitution (i.e., increase in d-spacing).

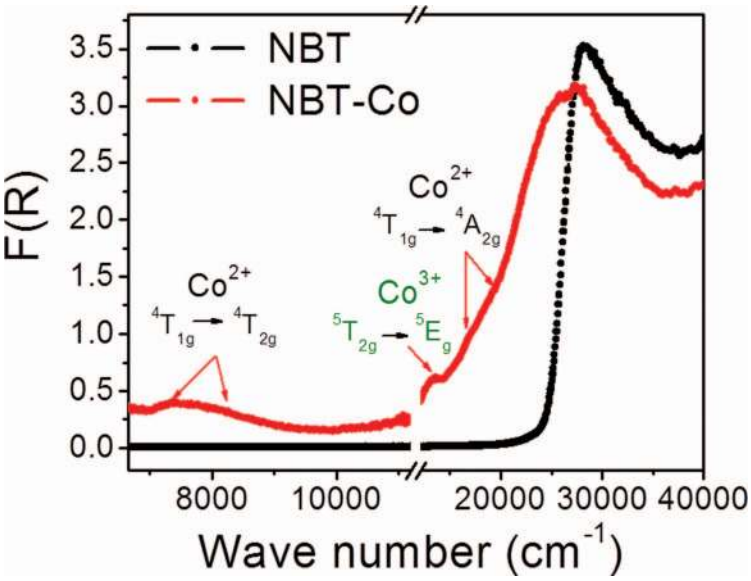

FIG. 2. Diffused reflectance spectra for NBT along with the corresponding octahedral crystal field transitions due to the presence of Co^{2+} and Co^{3+} - valence states in the NBT-Co sample.

states commonly in 2^+ and also in 3^+ oxidation states. Further studies to determine the oxidation state of the Co cation was carried out using solid state diffused reflectance spectroscopy (DRS).

The Kubelka-Munk (K-M) function, $F(R) = (1 - R)^2/2R$ (R – Reflectance) plotted as a function of wavenumber using the measured diffuse reflectance spectra of NBT and NBT-Co samples are shown in Fig. 2. The cobalt-ion substitution in the NBT lattice reflects a change in the DRS spectrum of NBT-Co sample as compared to NBT. On analyzing the spectra of NBT-Co sample, weak shoulders and bands were observed around ~16600 cm^{-1} and ~19200 cm^{-1}. These bands could be attributed to $^4T_{1g} \rightarrow {}^4A_{2g}$ and $^4T_{1g} \rightarrow {}^4T_{1g}(P)$ transitions of Co^{2+} (d^7) high spin (HS) octahedral complex.[25] Further, a weak band observed at ~14000 cm^{-1} could be attributed to $^5T_{2g} \rightarrow {}^5E_g$ transition of Co^{3+} (d^6-HS) ion. Along with these bands, a broad overlapped band centered at ~7300 cm^{-1} and ~8100 cm^{-1} belongs to $^4T_{1g} \rightarrow {}^4T_{2g}$ transition of Co^{2+} (d^7-HS) ion.[25] The spectroscopic studies

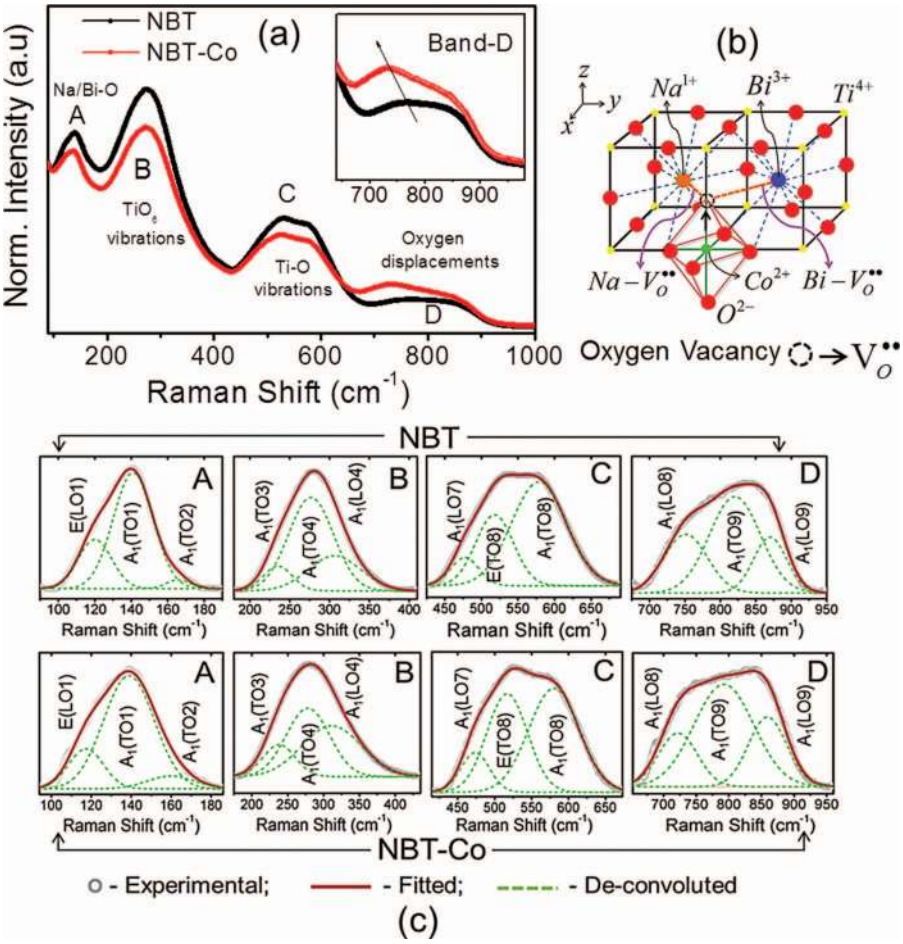

FIG. 3. (a) Raman scattering spectra for NBT and NBT-Co sample. Insets show the close observation of increase in the intensity and softening of phonon modes in band-D for NBT-Co sample. (b) Schematic representation of CoO_6 octahedra with formation of oxygen vacany ($V_O^{\bullet\bullet}$) and their associated bonds with respect to Na/Bi/Co-$V_O^{\bullet\bullet}$. (c) De-convoluted individual phonon modes for each band corresponding to NBT and NBT-Co sample.

clearly reveal the presence of mixed valence state (Co^{3+} & Co^{2+}) in the NBT-Co sample. However, the Co^{3+} is expected to be of relatively lower concentration in comparison to Co^{2+}. X-ray diffraction analysis also favors the aforementioned statement. Further, the non-existence of Co^{4+} state in NBT-Co system was evident from the absence of crystal field transitions corresponding to Co^{4+} (i.e., d^5 -ion).

The influence of Co-cation on the phonon modes of NBT-Co sample was further analyzed through Raman scattering studies. The Raman scattering spectrum of sintered NBT and NBT-Co samples were shown in Fig. 3(a). The observed Raman spectrum for NBT consists of several modes that are overlapped together and appear as four major bands which are depicted as band-A to band-D as shown in Fig. 3(a). In our recent work, a theoretical and experimental phonon mode analysis and their mode assignment has been carried out for NBT as follows:[9] band-A in the low frequency region centered around 135 cm^{-1} corresponds to A-O vibrations (i.e., Bi/Na-O); broad and highly intense band-B centered around 275 cm^{-1} corresponding to TiO_6 polyhedral vibrations; band–C were assigned to Ti-O vibrations; finally band-D in the high frequency region (i.e., 650 cm^{-1} to 950 cm^{-1}) has been assigned to oxygen displacements. Individual phonon modes in each band for both NBT and NBT-Co sample has been deconvoluted (see Fig. 3(c)) and their mode assignment has been tabulated (See Table I).

TABLE I. De-convoluted phonon modes of each band corresponding to NBT and NBT-Co sample and their mode assignment along with the difference in frequency shifts (Δ cm^{-1}) due to Co-substitution.

Phonon mode	E (LO1)	A_1 (TO1)	A_1 (TO2)	A_1 (TO3)	A_1 (TO4)	A_1 (LO4)	A_1 (LO7)	E (TO8)	A_1 (TO8)	A_1 (LO8)	A_1 (TO9)	A_1 (LO9)
NBT ***(cm^{-1})***	120	141	165	235	274	306	477.7	518	578.3	749.6	815.8	868.2
NBT−Co ***(cm^{-1})***	117	138.5	160	238	278.1	311	473.5	515.6	580	722.1	792.3	859.2
Δ ***cm^{-1}***	−3	−3	−5	+3	+3.1	+5	−4.2	−2.6	+1.7	**−27.5**	**−23.5**	**−9**

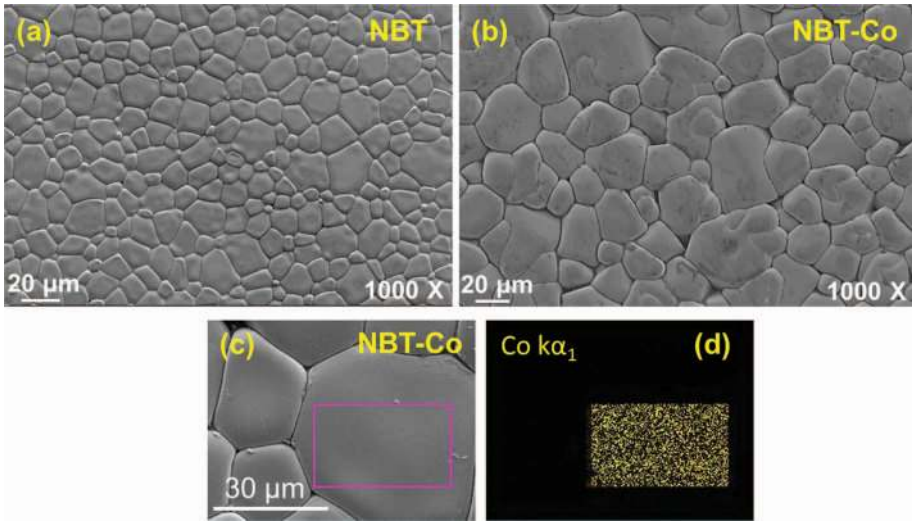

FIG. 4. FE-SEM micrographs of (a) NBT and (b) NBT-Co sample and their corresponding (c) & (d) elemental mapping on a selected area for NBT-Co sample.

A similar phonon spectrum observed for NBT-Co sample indicates that *R3c* symmetry is preserved. However, variation in intensity along with shift in the phonon modes were observed in NBT-Co sample. These changes in the phonon modes indicates the presence of structural distortion in NBT-Co system due to Co-ion substitution at Ti-site of the host NBT lattice. From the Raman spectra of NBT-Co sample, each band especially band-A, B & C suffers a suppression in the intensity of phonon mode. This could be attributed to the weakening of Na/Bi-O and Ti-O bonds in the vicinity of Co^{2+} substitution as shown in the schematic of Fig. 3(b). Further, a significant increase in the intensity of band-D and shift in the phonon mode towards lower frequency (i.e., softening) of about $\geq$20 cm^{-1} in certain phonon modes in NBT-Co sample clearly reveals the formation of oxygen vacancies $V_O^{\bullet\bullet}$ (i.e., 3-δ) and creates a defect state. A similar shift in phonon modes towards lower frequencies due to the formation of oxygen vacancies has been reported elsewhere.[26] In a similar manner, a slight frequency shift of $\cong$ 3–5 cm^{-1} were also observed in the phonon modes of band-A, B & C due to Co-substitution (See Table I). However, these frequency shift (cm^{-1}) is close to the resolution limit ($\cong$ 3 cm^{-1}) of our Raman spectrometer. Hence, we cannot explore the exact effect in these bands. In contrast, the strong frequency shift in band-D as stated above is well within the reslolution limit, hence we can strongly attribute this as an intrinsic contribution due to oxygen vacancies.

FE-SEM micrographs of the sintered NBT sample shows densely packed grains with an average grain size of $\cong$ 14 μm and NBT-Co sample shows $\cong$ 25 μm (See Fig. 4(a) and 4(b)). A significant grain growth in NBT-Co sample could plausibly be due to the formation of oxygen vacancies ($V_O^{\bullet\bullet}$), which acts a source for mass transport path and promotes long range solid state diffusion. This results in the exaggerated grain growth during sintering in NBT-Co sample.[27] Further, magnified region of

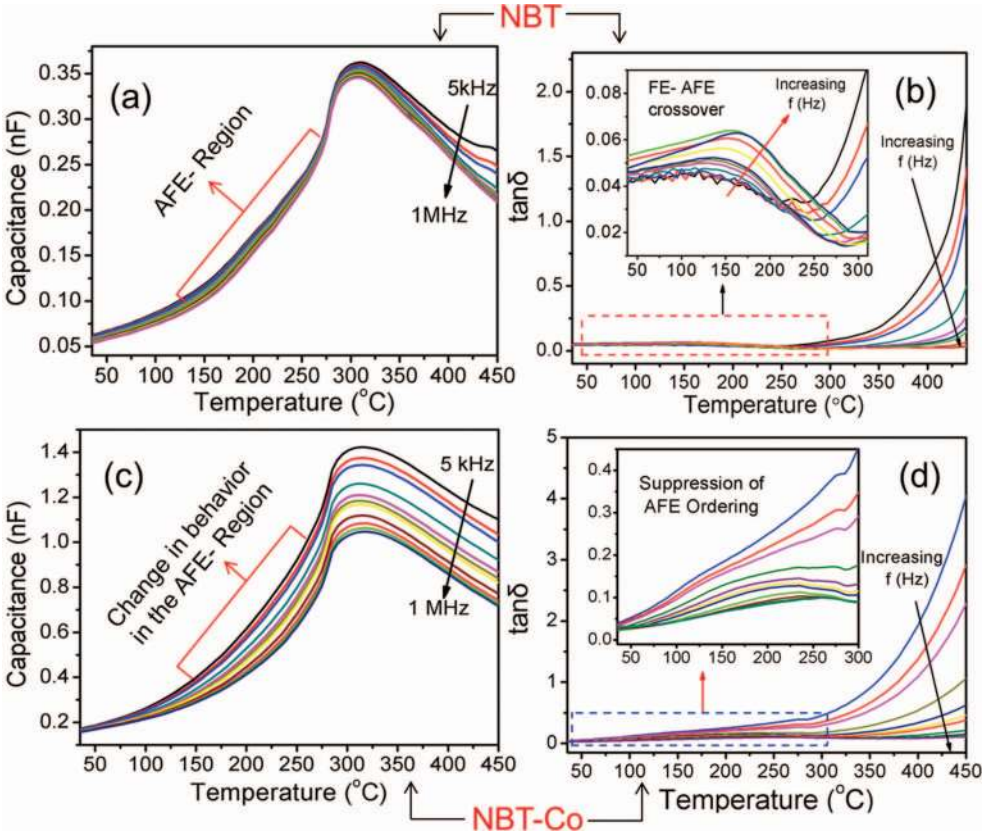

FIG. 5. Capacitance (C_P) vs T(°C) plots for (a) NBT and (c) NBT-Co sample indicating a change in the dielectric behavior across the AFE region. Temperature dependent tan δ vs. T(°C) for (b) NBT and (d) NBT-Co sample with inset showing the suppression of AFE ordering. (Applied bias voltage was 400 mV for both the samples).

NBT-Co sample depicts there is no any significant phase segregation at their grain boundaries as shown in Fig. 4(c). Along with this, elemental mapping of Cobalt (Co) in a selected region of a grain (See Fig. 4(d)) supports the uniform distribution of Co-ion in NBT-Co system.

A collective observations from x-ray diffraction, spectroscopic and microscopic studies, strongly reveals that Co-ion substitutes into the NBT lattice at Ti-site associated with the formation of oxygen vacancy as explained earlier. The major percentage of Co is in 2^+ oxidation state and in addition variation in lattice spacing and the increment in the unit cell volume perceives the homogenous distribution of Co-ion in the host NBT lattice. In order to analyze the ferroelectric phase transition behavior, both NBT and NBT-Co were further subjected to high temperature dielectric studies.

Temperature dependences of the capacitance (C_p) and tan δ with frequency variation from 5 KHz to 1 MHz for NBT and NBT-Co samples were shown in Fig. 5(a)–5(d). C_p vs. T(°C) plot for NBT ceramics depicts a steady increase in C_p with temperature and a slope change occurs in the intermediate temperature region (i.e.,1560 °C–280 °C). Similarly, in the intermediate temperature region a strong anomaly along with frequency dispersion was observed in the tan δ vs. T(°C) plot (see Fig. 5(b)). This intermediate region corresponds to the antiferroelectric (AFE) region,[6] where both ferroelectric (FE) and AFE behavior co-exist with FE dominance in the low-T region (150 °C–200 °C) and AFE dominance in the higher-T region (≥200 °C–280 °C).[8] After 280 °C, C_P increases until T_{max} with a broad dispersion and then C_p decreases further with increase in T(°C) corresponds to the AFE to paraelectric (PE) transition.[6,8] A similar behavior was observed in NBT ceramics by several authors.[6–9]

In this context upon cobalt-ion substitution in NBT, a significant change in the dielectric behavior was observed in both C_p vs. T °C and tan δ vs. T °C across the AFE region (see Fig. 5(c) and 5(d)). The steady increase in C_p without any slope change until T_{max} and suppression of the anomaly in the

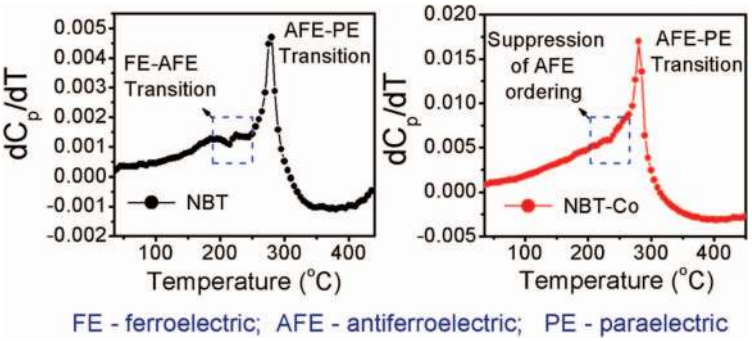

FIG. 6. The variation in dC_p/dTas a function of T(°C) plot for (a) NBT and (b) NBT-Co sample indicating the suppression of AFE ordering due to Co-substituion (*100kHz data was depicted for both the samples*).

tan δ (See inset of Fig. 5(d)) attributes the AFE ordering in NBT ceramic system was suppressed upon cobalt-ion substitution. Further, dC_p/dT vs. T(°C) plot (See Fig. 6(a) and 6(b)) depicts a suppression in anomaly for NBT-Co sample as compared to NBT sample around the FE-AFE transition shown in the encircled region of Fig. 6(b). This further supports the possibility of suppression in AFE ordeing for NBT-Co sample.

The reason for the suppression of intermediate AFE ordering in NBT-Co system can be described as follows: In NBT system, several electron diffraction reports evidenced that above 200 °C, there is a modulated phase (i.e., a planar defect) co-exist along within the *R3c* ($a^-a^-a^-$) matrix.[13,14,28] This modulated *Pnma* phase formation occurs mainly due to strain fluctuation in the oxygen octahedra. The stabilized modulated phase was found to be of intergrown orthorhombic *Pnma* sheets ($a^-b^+a^-$) between the *R3c* blocks (i.e., TiO_6 polyhedra in *R3c* phase), which gives rise to the formation of twin planes. As the temperature increases beyond 200 °C, more twins appear *Pnma* sheets) with reduced *R3c* blocks.[13,14] In the modulated phase the cations are displaced out of the cavity along $[u0w]_P$, hence the polar vectors reorient within in the *R3c* blocks. Due to twinning, the polar vectors between two succesive *R3c* block orient in opposite directions through a twin plane perpendicular to the modulated direction.[13,14] This gives rise to the AFE ordering in NBT system, which corresponds to the observation of anomaly in the dielectric behavior i.e., in the AFE region (See Fig. 5(a) and 5(b)). In NBT-Co system due to the oxygen vaccancies ($V_O^{\bullet\bullet}$) created by the defect state, the strain fluctuation in the oxygen octahedra is not sufficient to modulated the *R3c* blocks. As a consequence the phase modulated orthorhombic *Pnma* phase formation (twin plane) does not occur until T_{max}. This succeeds to the suppression of antiferroelerctric ordering in NBT-Co system as evidenced from the temperature dependent dielectric plots (see Fig. 5(c) and 5(d)). From the above discussions it is evident that stoichiometry (especially oxygen)/compositional fluctuation can suppress the formation of such modulated phase in NBT system.

A ferroelectric (P-E) hysteresis measurement (See Fig. 7(a)) depicts a well saturated loop with high P_r and coercivity (E_C) values for both NBT and NBT-Co sample. The sharp non-linear switching I-V curves for both the samplesshows their intrinsic FE character (See Fig. 7(b)). It is observed from PE-hysteresis loops that, there is no significant change in polarization values in both the samples (i.e, $\pm P_r/2 \cong 38\ \mu C/cm^2$). Howevr, increase in the coercive field ($E_C \cong 9$ kV/cm i.e., $E_C = \pm E_C/2$) value for NBT-Co sample (i.e., NBT-Co: $E_C \cong 71$ kV/cm; NBT: $E_C \cong 62$ kV/cm) indicates the hardening mechanism in NBT-Co sample. This, behavior further supports Co^{2+}-ion substitution in the host NBT lattice and acts as an acceptor type functional center.[24,29] As a consequence a defect complex is created by the formation of oxygen vacancies ($V_O^{\bullet\bullet}$) for charge compensation (Co_{Ti}'') as discussed earlier.

These defect complexes form an electrically neutral dipole P_D= q.l withq = +2e at the oxygen vacancy site and q = −2e at Co^{2+} site.[30] The neutral defect dipole can be represented as $P_D = (Co_{Ti}'' - V_O^{\bullet\bullet})^{\times}$ as shown in the schematic of Fig. 7(c). This neutral defect dipole may align parallel to the overall spontaneous polarization P_s direction (i.e., along pseudo-cubic body diagonal [111]), which leads to the unchanged macroscopic polarization values in NBT-Co sample.[29–31]

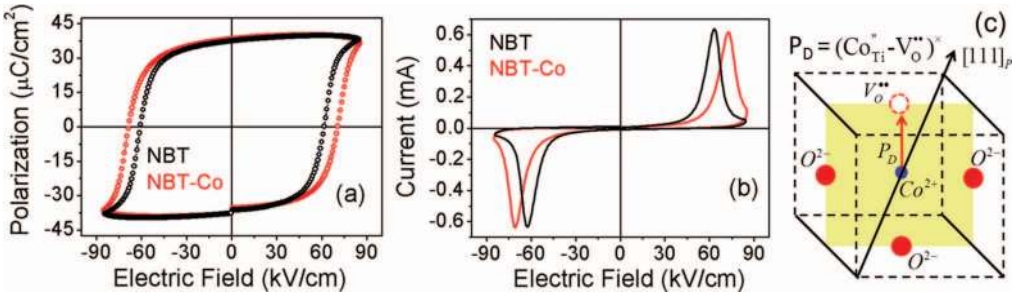

FIG. 7. Room temperature (a) P-E Hysteresis loops for NBT and NBT-Co samples measured until their dielectric breakdown at an applied frequency of 1 Hz and their associated (b) Current (I) - Voltage (V) switching curves. (c) Schematic representation of the orientation of neutral defect dipole (P_D) along with the direction of spontaneous polarization (P_S) for rhombohedral NBT-Co system.

However, these defect complexes orienting along the polarization direction acts as a pinning site and hinders the polarization switching (i.e., reversal). This inturn leads to the increase in coercivity values (i.e., hardening mechanism) in NBT-Co sample.[32]

IV. CONCLUSIONS

In summary, we conclude that Co-ion substitution at Ti-site of NBT host lattice most preferably stabilizes at Co^{2+} state and increases the unit cell volume along with creation of oxygen vacancies. This in-turn leads to the formation of neutral defect dipole $P_D = (Co_{Ti}^{''} - V_O^{\bullet\bullet})^{\times}$. These defect dipole act as a pinning site for domain reversal during polarization switching and harden the system with increasing coercivity (i.e E_C) values. Further, Co-substitution suppresses the intermediate AFE-ordering, by imparting the formation of modulated phase (i.e., *Pnma* phase). However, other high temperature structural and microscopic (TEM) investigations could exactly give us the exact nature and reason for AFE suppression in NBT-Co system and such studies are under progress.

ACKNOWLEDGMENTS

Dr. Saket Asthana gratefully acknowledge the financial support funded by Defence Research and Development Organization (DRDO), India under the project ERIP/ER/0900373/M/01/1430.

[1] Yet-Ming Chiang, Gregory W. Farrey, and Andrey N. Soukhojak, Appl. Phys. Lett. **73**, 3683 (1998).
[2] Jurgen Rodel, Wook Jo, Klaus T. P. Seifert, Torsten Granzow, and Dragan Damjanovic, J. Am. Ceram. Soc. **92**, 1153 (2009).
[3] G. A. Samara, Solid State Phys. **56**, 239 (2001).
[4] G. O. Jones and P. A. Thomas, Acta Cryst. B **58**, 168 (2002).
[5] Wenwei Ge, Jiefang Li, Dwight Viehland, and Haosu Luo, J. Am. Ceram. Soc. **93**(5) 1372 (2010).
[6] C. S. Tu, I. G. Siny, and V. H. Schmidt, Phys. Rev. B. **49**, 17 (1994).
[7] M. Matsuura, H. Iida, K. Hirota, K. Ohwada, Y. Noguchi, and M. Miyayama, Phys. Rev. B. **87**, 064109 (2013).
[8] Yuji Hiruma, Hajime Nagata, and Tadashi Takenaka, J. Appl. Phys. **105**, 084112 (2009).
[9] M. K. Niranjan, T. Karthik, S. Asthana, Jayasree Pan, and U. V. Waghmare, J. Appl. Phys. **113**, 194106 (2013).
[10] J. Kreisel, P. Bouvier, B. Dkhil, P. A. Thomas, A. M. Glazer, T. R. Welberry, B. Chaabane, and M. Mezouar, Phys. Rev. B. **68**, 014113 (2003).
[11] Jung-Kun Lee, Jae Yun Yi, and Kug Sun Hong, J. Appl. Phys. **96**, 1174 (2004).
[12] Jae Yun Lee and Jung-Kun Lee, J. Phys. D: Appl. Phys. **44**, 415302 (2011).
[13] V. Dorcet, G. Trolliard, and P. Boullay, Chem. Mater. **20**, 5061 (2008).
[14] V. Dorcet, G. Trolliard, and P. Boullay, J. Magn. Magn. Mater. **321**, 1758 (2009).
[15] Elena Aksel, Jennifer S. Forrester, Jacob L. Jones, Pam A. Thomas, Katharine Page, and Matthew R. Suchomel, Appl. Phys. Lett. **98**, 152901 (2011).
[16] Badari Narayana Rao and Rajeev Ranjan, Phys. Rev. B **86**, 134103 (2012).
[17] Badari Narayana Rao, Andy N. Fitch, and Rajeev Ranjan, Phys. Rev. B **87**, 060102 (2013).
[18] Elena Aksel, Jennifer S. Forrester, Benjamin Kowalski, Jacob L. Jones, and Pam A. Thomas, Appl. Phys. Lett. **99**, 222901 (2011).
[19] Elena Aksel, Jennifer S. Forrester, Benjamin Kowalski, Marco Deluca, Dragan Damjanovic, and Jacob L. Jones, Phys. Rev. B. **85**, 024121 (2012).

[20] Jianjun Yao, Wenwei Ge, Li Yan, William T. Reynolds, Jiefang Li *et al.*, J. Appl. Phys. **111**, 064109 (2012).
[21] J. Rodrigues-Carvajal, *FULLPROF. A Rietveld Refinement and Pattern Matching Analysis Program* (Laboratoire Leon Brillouin, CEA-CNRS, France, 2000).
[22] L. B. McCusker, R. B. Von Dreele, D. E. Cox, D. Louer, and P. Scardi, J. Appl. Cryst. **32**, 36 (1999).
[23] Puspendu Barik, Atanu Jana, and Tapas Kumar Kundu, J. Am. Ceram. Soc. **94**, 2119 (2011).
[24] Elena Aksel, Peter Jakes, Emre Erdem, Donald M. Smyth, Andrew Ozarowski, Johan van Tol, Jacob L. Jones, and Rudiger-A. Eichel, J. Am. Ceram. Soc. **94**, 1363 (2011).
[25] J. D. Lee, *Concise InorganicChemistry* (Oxford university press, 2010) 5th edition.
[26] Rachna Selvamani, Gurvinderjit Singh, Vasant Sathe, V. S. Tiwari, and P. K. Gupta, J. Phys.: Condens. Matter. **23**, 055901 (2011).
[27] Suk-Joong L. Kang, *Sintering-Densification, GrainGrowth and Microstructure* (Elseiver Publications, 2005).
[28] R. Beanland and P. A. Thomas, Scripta Materialia **65**, 440 (2011).
[29] Elena Aksel, Emre Erdem, Peter Jakes, Jacob L. Jones, and Rudiger-A. Eichel, Appl. Phys. Lett. **97**, 012903 (2010).
[30] Rudiger-A. Eichel, Ebru Erunal, Michael D. Drahus, Donald M. Smyth, Johan van Tol, Jerome Acker, Hans Kungl, and Michael J. Hoffmannd, Phys. Chem. Chem. Phys. **11**, 8698 (2009).
[31] Rudiger-A. Eichel, Paul Erhart, Petra Traskelin, Karsten Albe, Hans Kungl, and Michael J. Hoffmann, Phy. Rev. Lett. **100**, 095504 (2008).
[32] Kenji Uchino, *Ferroelectric Devices* (Marcel Dekker, Inc., Newyork, 2000).